Macromolecular Research

Article

DOI 10.1007/s13233-019-7052-1

www.springer.com/13233 pISSN 1598-5032 eISSN 2092-7673

Non-Isothermal Crystallization and Degradation Kinetic Studies of Synthesized Mo-TG end Capped Poly(ε-Caprolactone)

Sehar Mahalakshmi[1]
Thangevel Alagesan[2]
Vellaichamy Parthasarathy*[,3]
Ramasamy Anbarasan[4]

[1] Department of Physics, Anand Institute of Higher Technology, Kazhipattur - 603 103, Chennai, Tamilnadu, India
[2] Department of Physics, Presidency College, Chennai - 600 005, Tamilnadu, India
[3] Department of Physics, Hindustan Institute of Technology and Science, Padur - 603 103, Chennai, Tamilnadu, India
[4] Department of Chemical Engineering, National Taiwan University, Taipei - 10617, Taiwan

Received July 19, 2018 / Revised August 21, 2018 / Accepted September 16, 2018

Abstract: The molybdenum thioglycolate (Mo-TG) end capped poly(ε-caprolactone) (PCL) was prepared in the presence of novel Mo-TG nanohybrid initiator by ring opening polymerization (ROP) technique. The structural analysis was carried out by FTIR, ^{1}H and ^{13}C NMR techniques for the synthesized PCL. The particle size of the end capped Mo-TG nano hybrid in the PCL matrix was analysed by HRTEM. The morphology, surface roughness and average surface roughness of the polymer sample were investigated by AFM. The geometry of the nucleated crystals of PCL was examined using polarized optical microscopy (POM). The crystallization and thermal history of the sample under non-isothermal condition were assessed by DSC and TGA. The morphology of the nucleated crystals was analysed theoretically with the help of kinetic models for Mo-TG end capped PCL under non-isothermal crystallization condition. The kinetic parameters associated with crystallization and degradation processes of PCL were also determined using various kinetic models.

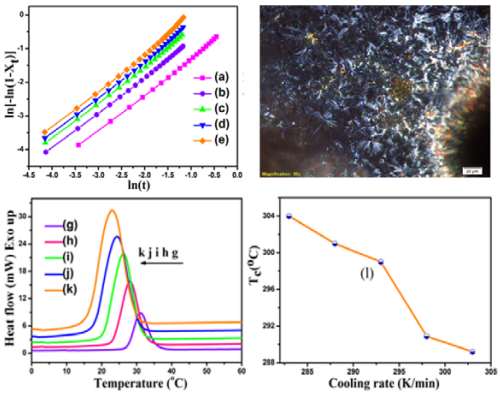

Keywords: PCL, crystallization, degradation, spherulite, AFM, POM.

1. Introduction

The importance of utilizing bio-degradable polymers has been increased worldwide in the biomedical field as well as in the packaging sectors, and also by considering the serious environmental problems caused by the petroleum based polymers in the landfill. The aliphatic polyesters are known as an important class of biodegradable or bioresorbable environmental friendly polymers. Polylactide, polyglycolate and poly(ε-caprolactone) are some of the widely used synthetic polyester in the biomedical and pharmaceutical applications.[1] Among these polymers, PCL is a promising synthetic biodegradable polyesters due to its biodegradability, biocompatibility and good material properties.[2,3] It finds major applications in implants, sutures, controlled drug delivery, tissue engineering, packaging and agricultural sectors.[4,5] The biodegradable PCL can be synthesized by two ways such as polycondensation of 6-hydroxyhexanoic acid and the ROP of caprolactone (CL).[6] The ROP of CL is more viable method to prepare PCL with higher molecular weight and lower polydispersity than poly condensation technique. The metal alkoxides with different metal ions such as aluminium (III) tert-butoxide, lithium tert-butoxide, tin (II) tert-butoxide and titanium (IV) tert-butoxide were reported as an initiator for the ROP of CL in the literature.[7] The ROP of CL was carried out in the presence of organolanthanide thiolate complexes by Sun *et al.*[8] The various chemical initiators namely calcium mercaptosuccinate,[9] Schiff base metal complex,[10] samarium acetate,[11] montmorillonite,[12] monomethoxy polyethylene glycol,[13] methanol,[14] isopropanol[15] were used towards ROP of CL. The thioglycolic acid decorated molybdenum nanoparticle (Mo-TG) was synthesized for this study. The synthesized Mo-TG nanoparticle has not been documented as an initiator for ROP of CL in the literature so far. This is the first time, Mo-TG end capped PCL was synthesized by using Mo-TG initiator in the presence of stannous octoate (SO) catalyst. The understanding of non-isothermal crystallization behaviour and the associated morphology of PCL is one of the most important factors to develop materials with some unique properties for particular applications. The crystallization mechanism of PCL/graphene oxide composite was examined under both isothermal and non-isothermal conditions.[16,17] The study revealed that the microstructure of the PCL composite was disturbed by the excess loading of graphene oxide in its matrix. Recently, the non-isothermal crystallization kinetic study on PCL and PCL-glass composite was carried out to investigate their crystallization process using kinetic models.[18] The PCL composites with starch and bamboo fibre were studied under non-isothermal condition to comprehend the physical and chemical changes associated with the crystallization process.[19] Chuang *et al.* studied the crystallization process of PCL/PEG blends.[20] The crystallization mechanism of silk-fibroin-fiber reinforced PCL biocomposite

***Corresponding Author:** V. Parthasarathy (parthu0406@gmail.com)

was reported by Qiao *et al.*[21] under different heating rates. The biodegradable PCL is mostly used in biomedical field and food packing industries. It undergoes slight degradation during an industrial process under non-isothermal condition which also affects the material's properties. Hence, the understanding of thermal degradation mechanism of PCL and its composites under non-isothermal condition is much more important to channelize them towards particular applications. The non-isothermal degradation kinetics of PCL was employed to assess its thermal degradation mechanism and the associated kinetic parameters.[22] The thermal degradation of PCL was performed under both isothermal and non-isothermal conditions using Friedman and Chang models.[23] The thermal degradation of aliphatic polyester was analysed with the help of isoconversional and model-fitting methods.[24] Chrissafis and his co-workers[25] prepared PCL composites with four different nanoparticles. All the prepared samples were investigated to assess their thermal degradation mechanism under non-isothermal conditions. The energy of activation for the degradation process was calculated using various kinetic models. The available reports showed that there were no similar studies with Mo-TG end capped PCL composite. Hence, the novelty of the present investigation is to carry out non-isothermal crystallization and degradation kinetic studies for the synthesized Mo-TG end capped PCL as these characteristics are more responsible for thermal processing, recycling and applications of PCL. The newly prepared Mo-TG initiator is not only acting as an initiator for the ROP of CL, it also acts as a nucleating agent. But, the decrease in T_c in DSC thermograms can be explained on the basis of restriction in segmental mobility and semi-crystalline nature of PCL.

2. Experimental procedure

2.1. Materials

The monomer, ε-caprolactone (CL) was procured from Merck, India for the preparation of PCL. Molybdenum carbonate and thioglycolic acid used for the preparation of Mo-TG nanoparticle were supplied by Aldrich, India. The other chemicals such as stannous octoate (catalyst, SO), diethyl ether and chloroform ($CHCl_3$) used for this work were purchased from Ottokemi, India.

2.2. Synthesis of Mo-TG nanohybrid

The starting materials for the preparation of Mo-TG nanoparticles were molybdenum carbonate and thioglycolic acid. The aqueous solution of $MoCO_3$ was prepared in 100 mL double distilled water. Then, it was mixed with 150 mL aqueous solution of thioglycolic acid under stirring in an inert atmosphere to initiate the chemical reaction. The precipitation of Mo-TG nanoparticle was formed at the end of the reaction. Afterwards, the obtained precipitate was filtered out and washed with distilled water. Then, it was kept in an oven at 100 °C for drying.

2.3. Synthesis of Mo-TG nanoparticles end capped PCL

The monomer CL was taken along with the newly prepared Mo-TG initiator and SO catalyst in a thermal reactor to initiate ROP of CL. The reaction mixture was stirred for about 15 min at 30 °C in the nitrogen environment. Then, it was placed in an oil bath at 160 °C for 2h. The highly viscous product was obtained at the end of the reaction and that was dissolved in 15 mL of $CHCl_3$. Afterwards, it was poured into 200 mL of diethyl ether where the Mo-TG end capped PCL was precipitated. Thus, the obtained polymer precipitate was filtered and dried at 45 °C in vacuum oven.

2.4. Characterization of the sample

The physical and chemical properties of Mo-TG end capped PCL were analysed with the help of analytical instruments. FTIR is a very useful analytical tool to confirm the structure of the materials. The synthesized PCL was made as a thin pellet by mixing it with KBr for this analysis. FTIR spectrum was recorded for the prepared pellet in the range of 400 to 4000 cm^{-1} using Shimadzu 8400S spectrometer, Japan. The ^1H and ^{13}C spectra were also recorded on Bruker Biospin high resolution digital 300 MHz NMR spectrometer, USA for confirming the structure of PCL in order to support the FTIR's result. The surface topography of the PCL composites was evaluated with the help of Park XE7 atomic force microscope. The particle size of the incorporated Mo-TG nanoparticle and the morphology of the PCL were analysed using JEOL 2100 tunnelling electron microscope (TEM). The microstructure of the nucleated polymer crystals during the crystallization process was captured using Olympus BX51 polarized optical microscope. The crystallization and the melting behaviour of PCL composite were investigated under non-isothermal condition with the help of Toledo DSC 822e differential scanning calorimeter (DSC). The data obtained from TG/DTA 6200 thermal analyser were used to assess the thermal stability and thermal degradation process of the sample under non-isothermal condition.

2.5. Non-isothermal crystallization kinetics

The theoretical determination of the nucleated crystals and their morphology were determined under non-isothermal condition by using the data obtained from DSC. The heat release during the crystallization process of polymer can be measured by DSC. It is very clear that the evolution of crystallinity is associated with the released heat. Hence, the relative crystallinity (X_t) is expressed as a function of crystallization temperature by the following equation:[26]

$$X_t = \frac{\int_{T_0}^{T} \frac{dH_c}{dT} dT}{\int_{T_0}^{T_\infty} \frac{dH_c}{dT} dT} \quad (1)$$

where dH_c is the enthalpy of crystallization at an infinitesimal time interval dt. T_0 and T_∞ are the onset and end temperatures of the crystallization respectively. The Avrami equation based model is employed to describe the crystallization parameters as well as the propagating nucleation under non-isothermal condition for the Mo-TG end capped PCL. The Avrami expres-

sion is proposed below:[27]

$$1-X_t = \exp(-Z_t t^n) \quad (2)$$

where X_t stands for relative crystallinity at crystallization time, n is the Avrami exponent and Z_t describes the crystallization rate constant. The nucleation and growth mechanism of crystals are dependent on the values of n and Z_t. The Eq. (2) can also be written in the following form:

$$\ln[-\ln(1-X_t)] = \ln Z_t + n \ln t \quad (3)$$

The non-isothermal crystallization mechanism of PCL composite was also examined by the combined Avrami and Ozawa model. It proposes the following expression:[28]

$$\log(\Phi) = \log F(T) - b\log(t) \quad (4)$$

where Φ represents the cooling rate, $F(T)$ is crystallization rate constant, t refers to crystallization time and b is Ozawa exponent. The terms $F(T)$ and b describe the nucleation and growth mechanism of the nucleated crystals.

The energy associated with the crystallization process can be described by the Kissinger model. The crystallization peak temperature (T_c) needs to be measured from the DSC curves at different cooling rates to make Kissinger plot.[29]

$$\frac{d\left[\log\left(\frac{\varphi}{T_C^2}\right)\right]}{d\left(\frac{1}{T_c}\right)} = \frac{E_a}{R} \quad (5)$$

The following equation is obtained by integrating Eq. (5),

$$\log\left(\frac{\varphi}{T_c^2}\right) = \frac{E_a}{R}\frac{1}{T_c} \quad (6)$$

where E_a is the energy of activation, R denotes the universal gas constant, T_c is the crystallization peak temperature at which reaction rate reaches maximum and φ is the cooling rate.

2.6. Non-isothermal degradation kinetics

The thermal degradation mechanism of Mo-TG end capped PCL was analysed under non-isothermal condition to evaluate the activation energy using the isoconversional and model fitting kinetic models. The reaction conversion (α) for the degradation process is expressed by the following mathematical expression:[30]

$$\alpha = \frac{W_o - W_t}{W - W_f} \quad (7)$$

where W_o and W_f are the initial and final weights of the sample, and W_t is the weight at any temperature.

2.6.1. Flynn-Wall-Ozawa method

Flynn-Wall-Ozawa (FWO) kinetic model is one of the important isoconversional methods.[31] The degree of conversion (α) can be measured for the associated degradation temperature of the prepared samples under non-isothermal condition. The advantage of this model is determining the activation energy (E_a) without knowing the reaction mechanism.

$$E_a = \frac{-R}{1.052} \times \frac{\Delta\lambda\nu\beta}{\Delta(1/T)} \quad (8)$$

where E_a is an activation energy, β is the heating rate, R describes the gas constant and T is the temperature.

2.6.2. Kissinger model

It is a model fitting method. According to the Kissinger model, the rate of reaction reaches its maximum at the thermal degradation temperature (T_d). The degree of conversion (α) is considered to be constant at T_d for this model. However, it varies with the heating rate in many cases. The Kissinger model suggests the following logarithmic form of the expression:[32]

$$\ln\left(\frac{\beta}{T_d^2}\right) = \ln\left(\frac{AR}{E}\right) - \frac{E}{RT_d} \quad (9)$$

The activation energy can be calculated form the slope of the plot $\ln(\beta/T_d^2)$ *vs.* $1/T$.

2.6.3. Auggis-Bennet model

It is also known as model fitting method. Auggis and Bennet model[33] is used to determine the energy of activation (E_a) for thermal degradation process at different heating rates for Mo-TG end capped PCL. It suggests the following expression:

$$\ln\left(\frac{\beta}{T_d}\right) = -\frac{E}{RT_d} + \ln A \quad (10)$$

The degradation temperature (T_d) can be measured from the TGA thermograms at different heating rates and that will be used to make a plot of $\ln(\beta/T_d)$ vs. $1/T$ for evaluating the E_a values.

2.6.4. Friedman method

The Friedman model is a well-known differential iso-conversional method.[34] This model was developed from the degradation rate expression without any assumptions. It was modified with certain assumptions of other isoconversional expression for differential applications. The proposed logarithmic form of rate equation is given below:

$$\ln\left(\frac{d\alpha}{dt}\right) = \ln(Z) + n\ln(1-\alpha) - \frac{E_a}{R_1} \quad (11)$$

where R, α and T represent the gas constant, conversion rate at time t and temperature respectively.

3. Results and discussion

3.1. FTIR study

The FTIR spectrum of Mo-TG nanoparticle is illustrated in Figure 1(a). The peak at 3470 cm^{-1} refers to -OH stretching vibration. The C-H stretching and anti-symmetric stretching vibrations are found at 2855 cm^{-1} and 2937 cm^{-1} respectively. The carbonyl stretching vibration is assigned at 1718 cm^{-1}. The peak assigned at 1556 cm^{-1} is observed to be C-H bending vibration. The C-S and C-O-C stretching vibrations of TG are noticed at 1410 cm^{-1} and 1166 cm^{-1} respectively. The C-H out of plane bending vibration (OPBV) of TG is seen at 730 cm^{-1}. The peak at 628 cm^{-1} indi-

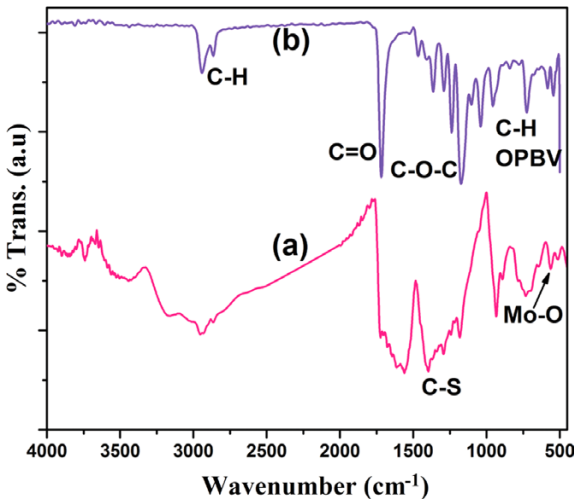

Figure 1. FTIR spectrum of (a)Mo-TG nanohybrid, (b)Mo-TG end capped PCL system.

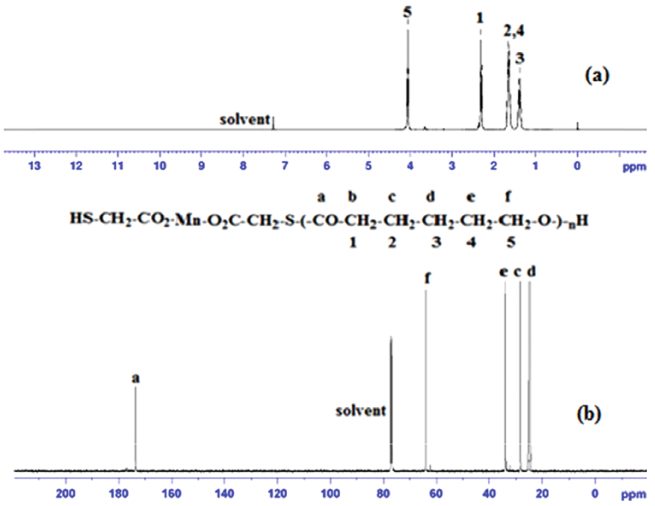

Figure 3. (A) ^{1}H NMR spectrum (B) ^{13}C NMR spectrum of Mo-TG end capped PCL.

cates the Mo-O stretching vibration. The FTIR spectrum of Mo-TG end capped PCL is shown in Figure 1(b). The emerging peaks at 2866 and 2942 cm^{-1} are referred to C-H symmetric and asymmetric stretching modes of PCL. The characteristics carbonyl stretching (C=O) mode of PCL is noticed at 1722 cm^{-1}.[28] The C-O-C stretching of PCL is appeared at 1183 cm^{-1}. The peak at 728 cm^{-1} is associated with the C-H out of plane bending vibration of PCL.[34] The structure of PCL was confirmed by the presence of C-H and C=O stretching peaks.

3.2. GPC analysis

Figure 2(a) and (b) represent the GPC profile of pristine PCL and Mo-TG end capped PCL. The obtained results revealed that the number average molecular weight (M_n) and weight average molecular weight (M_w) of Mo-TG end capped PCL were notably higher than pristine PCL. The rise in molecular weight of Mo-TG end capped PCL also confirmed the successful interaction of Mo-TG nano hybrid with the PCL matrix. The GPC data are given in Table 1.

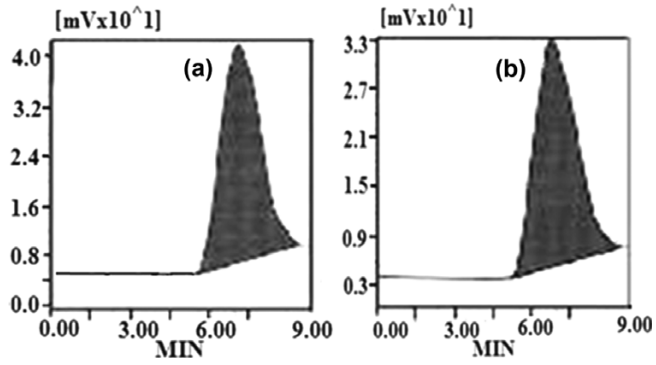

Figure 2. GPC profile of (a) pure PCL and (b) Mo-TG end capped PCL.

Table 1. GPC data of pure PCL and Mo-TG end capped PCL

System	M_n	M_w (g/mol)	P.D
PCL	11532	13682	1.18
PCL-Mo-TG	13108	14889	1.25

3.3. NMR study

The structure of Mo-TG end capped PCL was further verified with ^{1}H NMR and ^{13}C NMR spectra. Figure 3(a) represents the ^{1}H NMR spectrum of Mo-TG end capped PCL. The signal at 7.27 ppm attributes to the solvent ($CHCl_3$). The alkoxy proton peak is identified at 4.08 ppm in the ^{1}H NMR spectrum.[34] The signal for methylene proton situated near to the carbonyl group is observed at 2.32 ppm.[34] The other protons of PCL are emerged between 1.39 and 1.69 ppm. The structure of PCL was undoubtedly confirmed by the aforementioned peak. Figure 3(b) exhibits the ^{13}C NMR spectrum of Mo-TG end capped PCL. The solvent peaks are noticed between 76.7 and 77.4 ppm in the carbon NMR. The signal at 173.57 ppm is attributed to the carbon of carbonyl group in PCL. The peak at 64.1 ppm is related to the alkoxy carbon signal. The signal for methylene carbon adjacent to the carbonyl group of PCL is observed at 34.1 ppm.[34] All the assigned signals in carbon NMR spectrum are associated with the structure of Mo-TG end capped PCL.

3.4. HRTEM study

The morphology and particle size of the incorporated Mo-TG nano hybrid in PCL matrix were investigated by TEM. Figure 4(a) depicts the TEM image of Mo-TG end capped PCL. The presence of nano hybrid in the host matrix was witnessed from the micrograph. The fluffy white back ground of PCL is seen embedded with different size of Mo-TG nanoparticles in the TEM image. The morphology of the incorporated Mo-TG nanoparticles is in both spherical and irregular shape. The nano hybrid particles are interconnected with each other somewhere in the PCL matrix. Moreover, the size of the Mo-TG nanoparticles was measured in the range of >50 nm. This is indicated by the circled area. Some agglomerated Mo nanoparticle is also seen. The SAED pattern of Mo-TG end capped PCL is illustrated in Figure 4(b). The semi-crystalline nature of PCL was confirmed by the presence of concentric rings with dots.

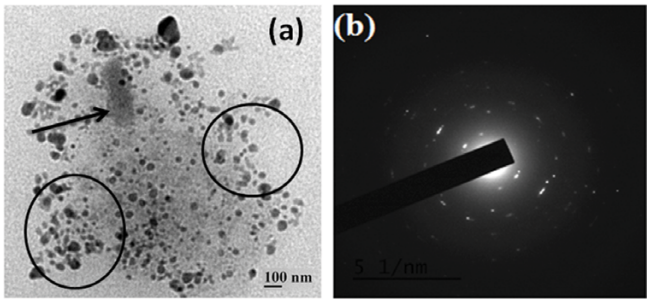

Figure 4. (a) HRTEM image and (b) SAED pattern of Mo-TG-PCL system.

3.5. AFM study

The functional performance of the materials mainly depends on the surface nature of the materials. The surface topography of the sample was visualized by AFM. The AFM micrographs of Mo-TG end capped PCL are shown in both 2D and 3D images (Figure 5(a) & (b)). The peak and valley profiles, surface roughness and grain orientation of the prepared sample were analysed with the help of typical AFM images. The interaction of nano hybrid with the PCL matrix was understood from the AFM images. The yellow rich regions obviously represent the PCL matrix. The grains notably seem to be in different shape, size and spacing. It is noted that PCL is a semi-crystalline polymer and the crystallinity can be induced by the Mo-TG. The crystals of PCL can be oriented in any direction. The crystal growth in a single direction leads to the smooth PCL surface. Figure 5(c) shows the AFM 3D image of Mo-TG end capped PCL. Here the surface of PCL is smooth and is indicated by the hill and valley peak height difference. The root mean square and average surface roughness were determined as 7 nm and 5 nm respectively from the 2D micrograph. The AFM micrograph shows both peaks and valleys. However, the surface has more planar regions which is confirmed by the negative skewness moment (-0.349). The height distribution of the peaks is probably symmetrical throughout the surface.

3.6. DSC profile

The DSC heating scan of pristine PCL heated at 10 °C/min is depicted in Figure 6. The T_m of pristine PCL was observed at

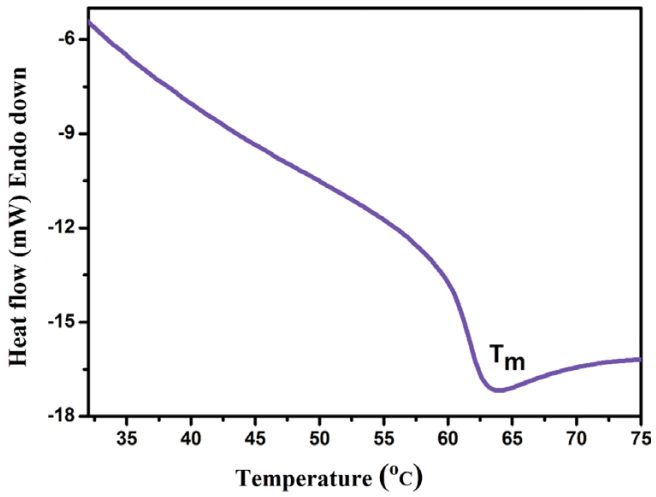

Figure 6. DSC heating scan of pure PCL.

62.7 °C, which was found to be lower (63.2 °C) than Mo-TG end capped PCL heated at the same heating rate. The crystallization and melting behaviour of PCL composite at different heating rates were examined by performing DSC analysis. The sample was heated from 10 to 30 °C/min in steps of 5 °C/min in the range of -30 °C to 100 °C under N_2 atmosphere. Figure 7(a)-(e) shows the DSC heating scan of Mo-TG end capped PCL. The T_m of PCL was found to be 60.8 °C for the sample heated at 10 °C/min. The T_m of PCL was noticeably shifted to higher temperature with the increasing heating rates. The similar observation was documented in the literature.[35] It was further confirmed from the plot of heating rate *vs.* T_m as shown in Figure 7(f). There was a linear increase in T_m with the increasing heating rates. The heat energy needed for melting the substance is possibly reduced at higher heating rates, which allows the polymer chains being relaxed during the fast scanning process. It concludes that T_m of PCL changes with the heating rate. At lower heating rates, the Mo-TG end capped PCL exhibited double T_m. This can be explained as follows: The first and foremost reason is difference in M_w of PCL. The PCL chains with slightly higher molecular weight exhibited the T_m slightly at higher temperature. The second possible reason is the PCL chains exist very closer to the Mo-TG is protected by the nano hybrid and resulting with slightly higher T_m value. The third least possible reason is the different crystalline

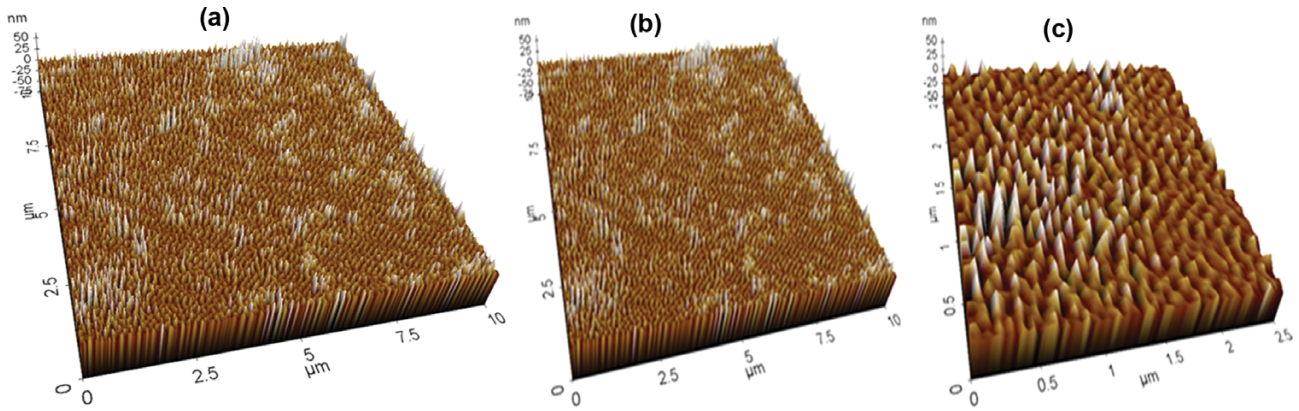

Figure 5. (a) 2D AFM image, (b) 3D AFM image (10 μm) (c) 3D AFM image (2.5 μm) of Mo-TG end capped PCL system.

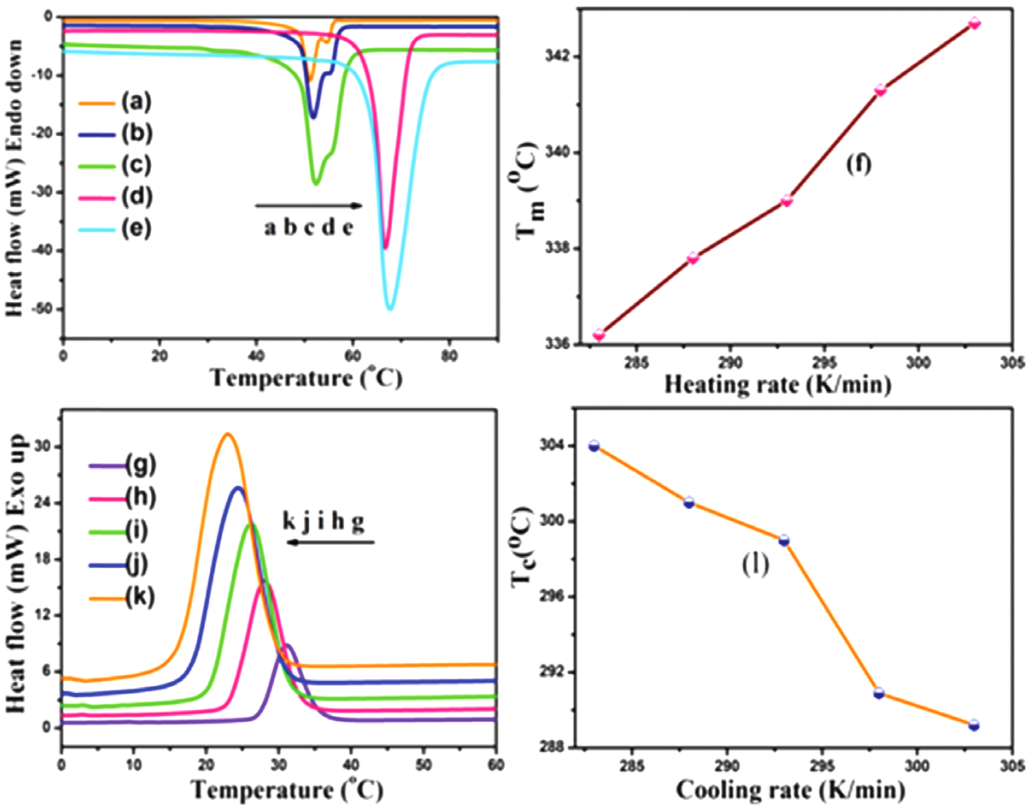

Figure 7. (a)-(e) DSC heating scan, (f) plot of heating rate against T_m, (g)-(k) cooling scan, (l) plot of cooling rate against T_c of Mo-TG end capped PCL system.

forms of PCL may have different T_m value. At lower heating rates, the PCL chains are slowly scanned and relaxed whereas at higher heating rates (for example from 25 to 30 °C/min) the PCL chains relaxed more and scanned fast. As a result, the PCL produced a single T_m at higher heating rates. Figure 7(g)-(k) displays the DSC cooling scan of PCL at five different cooling rates from 10 to 30 °C/min in steps of 5 °C/min in the same temperature range. The crystallization temperature of PCL was noted as 30 °C from the exothermic peak of the PCL sample cooled at 10 °C/min. The T_c value also decreases with the increasing cooling rates.[36] The plot of cooling rate against T_c confirms the same as shown in Figure 7(l). It was concluded that the T_c of PCL can be altered by changing the cooling rate. The data obtained from the DSC thermograms are listed in Table 2.

3.7. Non-isothermal crystallization study

The crystallization behaviour of Mo-TG end capped PCL was analysed to evaluate crystallization rate constant and nucleation mechanism with the aid of reliable mathematical models. The prepared sample was cooled at different cooling rates to record the exothermic curves in the temperature range of -30 °C to 100 °C. The exothermic curves recorded at different cooling rates are shown in Figure 7(g)-(k). The crystallinity (X_c), crystallization enthalpy (ΔH_c) and crystallization peak temperature (T_c) were derived from the exothermic curves of PCL for all the cooling rates. It was observed that the exothermic curves become wider and also the T_c value of PCL shifts towards lower temperature while increasing the cooling rates. The crystallization process takes place slowly at lower cooling rates. Hence, the crystallization occurs at higher temperature for lower cooling rates. The exothermic curves become wider at higher cooling rates since the crystallization process occurs under super cooling. The similar trend has been observed by many researchers.[37]

The nucleation mechanism and the growth geometry of the crystals were inspected under non-isothermal condition for the Mo-TG end capped PCL by using two different models. According to the Avrami expression (Eq. (3)), the plot of ln[-ln(1-X_t)]

Table 2. DSC data of Mo-TG end capped PCL system.

Heating rate (°C)	T_c (°C)	ΔH_c (Jg^{-1})	χ_c (%)	E_a (kJ/mol)	T_m (°C)	ΔH_m (Jg^{-1})	T (T_m-T_c) (°C)
10	31.0	55.8	41.0		63.2	58.1	32.2
15	28.0	56.2	41.3		64.8	58.1	36.8
20	26.0	57.3	42.1	198.2	66.0	86.9	40.0
25	17.9	59.7	43.8		68.3	61.9	50.4
30	16.2	61.5	45.2		69.7	94.1	53.5

c_c=($\Delta H_f/\Delta H_f^*$)×100, (ΔH_f^*=136 J/g).

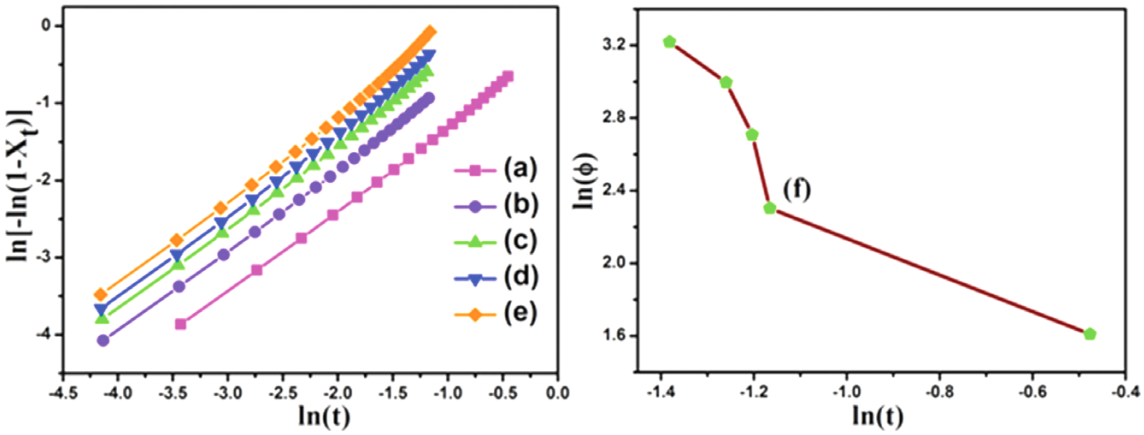

Figure 8. (a)-(e) Avrami plot for Mo-TG end capped PCL system at the cooling rates of 10, 15, 20, 25, 30 °C min^{-1}, and (f) Avrami-Ozawa plot.

vs. ln(*t*) (Figure 8(a)-(e)) gives a straight line from which Avrami exponent (*n*) and crystallization rate constant (Z_t) have been determined for all the five cooling rates. The n and Z_t values were measured from the slope and intercept of the above said plots. The n values are in the range of 2.83 to 3.86, which demonstrates that the grown crystals are in the 3D spherulitic shape.[38] The Z_t values were determined to be in the range 0.5 to 2.1 for various cooling rates. The crystallization rate increases with the increasing cooling rates. It was concluded that the crystallization time decreases with the increasing cooling rates since the crystallization rate constant is inversely proportional to crystallization time. The *n* and Z_t values are related to the rate of nuclei formation and spherulitic growth in Eq. (3). The combined Avrami and Ozawa model is also known as Mo's model which is given in Eq. (4). The reliability of the obtained crystallization parameters by Avrami model was further confirmed with Mo's model for the PCL composite. The terms $F(T)$ and *b* describe the nucleation and geometry of the grown crystal in this model. The plot of ln(Φ) *vs.* ln(*t*) was drawn to get the values of $F(T)$ and *b* as shown in Figure 8(f). The values of $F(T)$ and *b* were calculated as 1.66 and 3.8 respectively from the slope and intercept of the plots. The Ozawa exponent (b) is above 3 which also suggests the 3D spherulitic crystal growth.[38] The crystal structure was also confirmed with polarized optical microscope. The polarized optical micrograph is shown in Figure 9. The grown crystals are in the 3D spherulitic shape. The results of kinetic models were matched with the experimental results for the prepared PCL composites.

The Kissinger model was applied to calculate the required energy for the transportation of molecules from the molten state to an interface of growing crystal. The energy of activation (E_a) associated with the crystallization process under non-isothermal condition was calculated by this technique. Obviously, the plot of ln(Φ/T_c^2) *vs.* $1/T_c$ was drawn in order to obtain E_a value for PCL system as mentioned in Figure 10(a). The E_a value was evaluated as 198.2 kJ/mol. The obtained E_a value was remarkably higher than pure PCL.[33] It confirms that the incorporated Mo-TG hybrid acts as a nucleation agent which significantly enhances the transportation ability of polymer chains of PCL in the molten state resulting with higher E_a value. The crystallization rate coefficient (CRC) was estimated from the plot of crystallization temperature (T_c) as a function of cooling rate (Φ) as given in Figure 10(b). The slope value was determined as -0.794. The crystallization rate is generally higher for polymers of short repeating units rather than with longer or branched chains. Figure 10(c) shows a linear relationship between T_m and T_c.

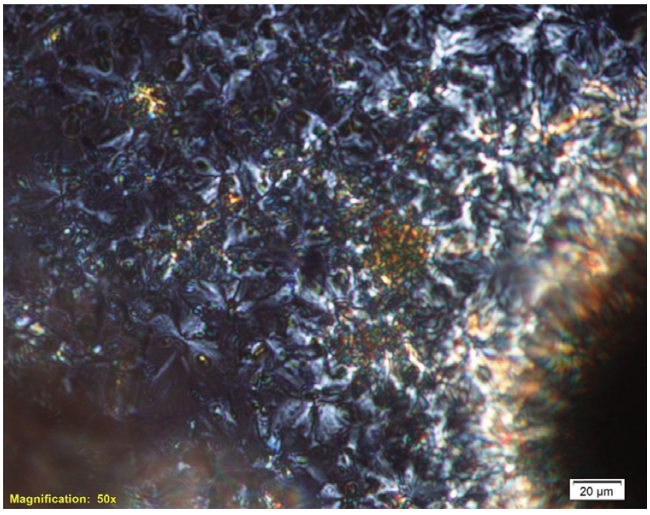

Figure 9. Polarized optical microscope image of Mo-TG end capped PCL system.

3.8. TGA profile

The TG thermograms of pristine PCL and Mo-TG end capped PCL are shown in Figure 11(a) and (b). A single step degradation process was observed for both the systems. The degradation temperatures of PCL and Mo-TG end capped PCL were measured as 393.4 °C and 392.5 °C respectively from the derivative curve. However, the residual mass obtained above 450 °C was higher (8.4%) for Mo-TG end capped PCL than pure PCL (4.8%). The thermal history of Mo-TG end capped PCL under non-isothermal condition was also recorded to understand its thermal degradation process. The sample was heated at five different heating rates in the temperature range of 30 °C to 600 °C in air atmosphere. The degradation study of PCL and Mo-TG end capped PCL was made under air atmosphere in order to maintain the natural environmental condition. The degradation study

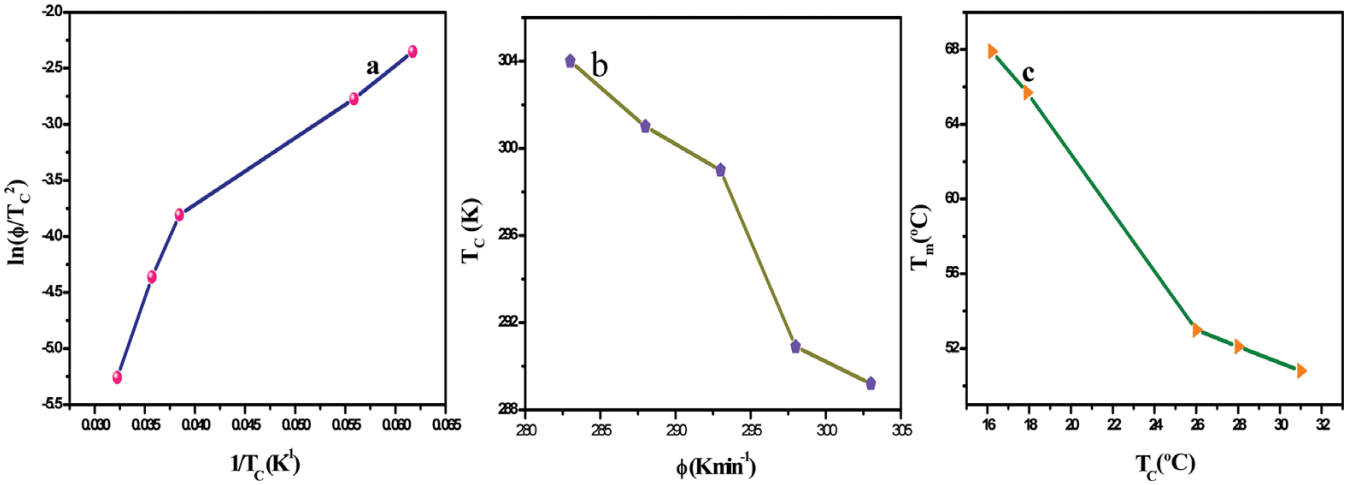

Figure 10. (a) Kissinger E_a plot (b) crystallization rate coefficient plot (c) the plot of T_m against T_c for Mo-TG end capped PCL system.

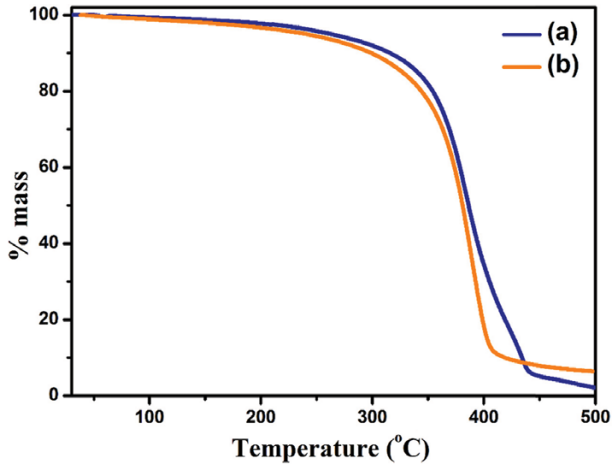

Figure 11. TGA thermogram of (a) pure PCL and (b) Mo-TG end capped PCL.

under nitrogen atmosphere will show higher degradation temperature than the natural air atmospheric condition. Figure 12(a)-(e) presents the TGA curves of PCL system for all five heating rates. All the thermograms exhibited the single step degradation process in the range of 240 °C to 418 °C for the PCL system which occurred due to the breaking of PCL backbone. The initial degradation temperature (T_{id}) was observed at 240 °C for the sample heated at 10 °C/min. However, it was remarkably shifted to higher temperature in accordance with the increasing heating rate. The final decomposition temperature was also shifted to higher temperature with the increasing heating rates. This is in accordance with the literature report.[39] The final degradation temperature (T_{fd}) of PCL was noticed at 389.4 °C for the sample heated at 10 °C/min, which was found to be increased with the increasing heating rate. The derivative thermograms of PCL for all the five heating rates are illustrated in Figure 12(f)-(j). The Differential thermograms (DTG) also revealed that there is an increasing trend in the degradation temperature (T_d) with the increasing heating rates. The PEMA-*co*-PHEMA-*g*-PCL system showed two step degradation processes with initial degradation temperatures at 243 °C and 361 °C respectively.[40] Hence, the Mo-TG end capped PCL system is thermally stable while compared with the reported one.

3.9. Non-isothermal degradation study

The kinetic parameters associated with degradation process under non-isothermal condition were determined by using the aforementioned models for Mo-TG end capped PCL. The polymer sample was heated at five different heating rates in air atmosphere to understand its thermal degradation mechanism. The

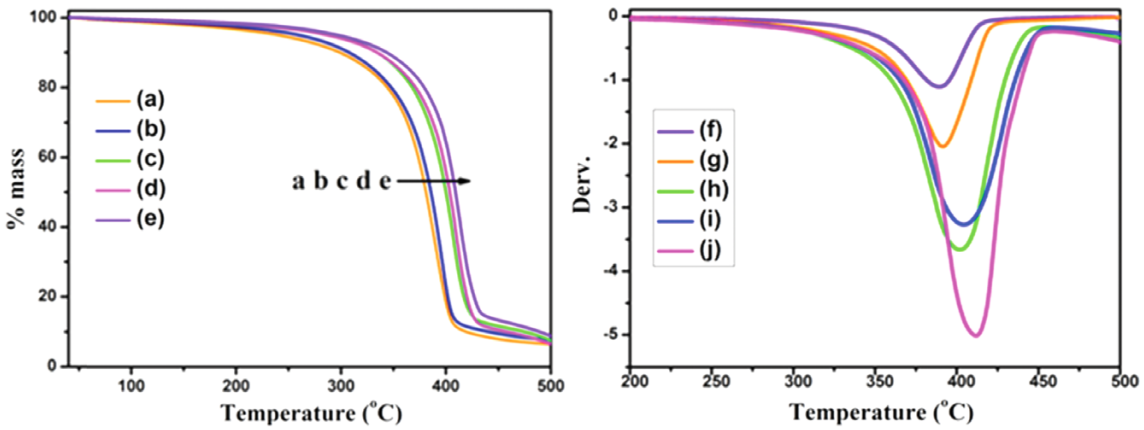

Figure 12. (a)-(e) TGA thermograms, (f)-(j) derivative thermograms of Mo-TG end capped PCL system at five different heating rates.

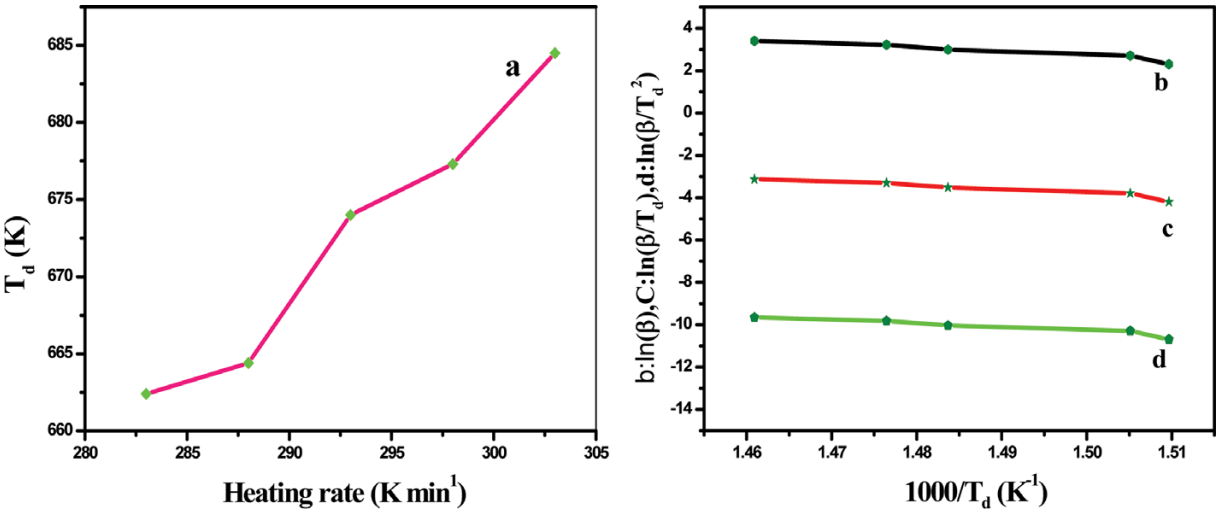

Figure 13. (a) Effect of heating rate on the T_d of Mo-TG end capped PCL system (b) Flynn-Wall-Ozawa plot (c) Auggis-Bennet plot (d) Kissinger plot for Mo-TG end capped PCL system.

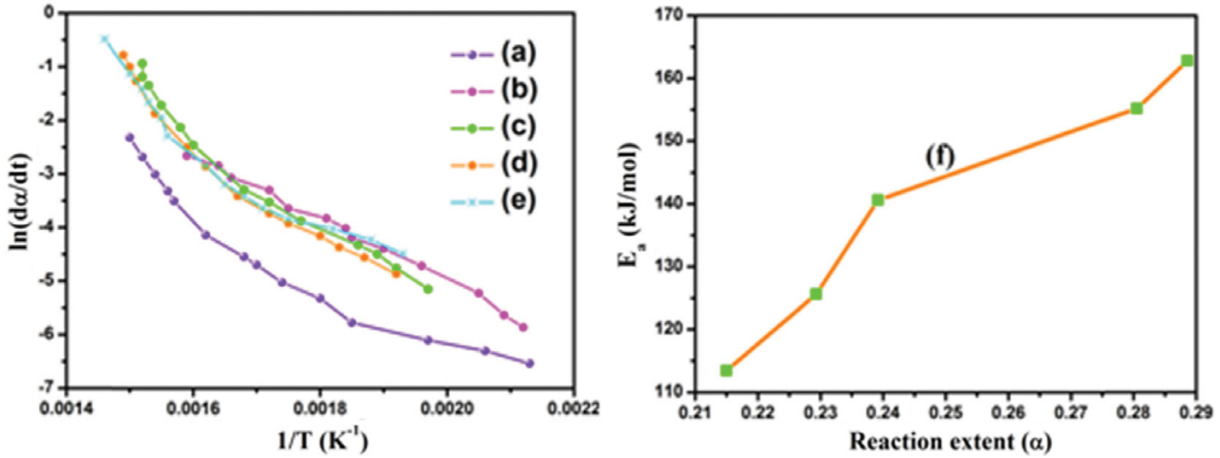

Figure 14. (a)-(e) Friedman plot for Mo-TG end capped PCL system at the heating rates of 10, 15, 20, 25, 30 °C min^{-1}, (f) plot of E_a against reaction extent.

TG patterns of Mo-TG end capped PCL and its derivative plots for all the five heating rates are given in Figure 12(a)-(e) and Figure 12(f)-(j) respectively. The increase in degradation temperature (T_d) was understood from the TG thermograms while increasing the heating rate. It was also observed that DTG curves become wider while increasing the heating rate.

The plot of T_d vs heating rate is shown in Figure 13(a). It shows that there is a gradual increase in the degradation temperature of PCL with the increasing heating rate. This is due to the fast scanning process. The methodology for finding the activation energy differs with different models. Flynn-Wall-Ozawa model (the plot of lnβ *vs.* 1000/T_d; Figure 13(b)), Auggis-Bennet method (the plot of ln(β/T_d) *vs.* 1000/T_d; Figure 13(c)) and Kissinger method (ln(β/T_d^2) *vs.* 1000/T_d; Figure 13(d)) were applied to find out the E_a values for the degradation of PCL under non-isothermal condition.[33] The E_a values were obtained to be 170.8 kJ mol^{-1} for FWO, 165.2 kJ mol^{-1} for Auggis-Bennet and 159.6 kJ mol^{-1} for Kissinger models respectively from the slope of the above said plots. The obtained E_a values are within the acceptable error limits. The lower E_a value was recorded only for Kissinger model. This is because of the denominator on Y-axis.

The Friedman method was also applied to find out the E_a value for non-isothermal degradation process of Mo-TG end capped PCL. The plot of ln($d\alpha/dt$) vs. 1/T (Figure 14(a)-(e)) was drawn to find out E_a according to this model. All the plots showed a decreasing trend. The obtained E_a values were calculated to be in the range of 113.4 to 162.8 kJ mol^{-1} for all the five heating rates. The plot of E_a *vs.* reaction extent (Figure 14(f)) shows a kind of linearity between them. It was reported that E_a values of pristine PCL for the degradation process were obtained as 171 kJ mol^{-1} and 177 kJ mol^{-1} by Kissinger and Friedman models.[30] However, these values were reported to be decreased once PCL blended with poly(trimethylene carbonate). Similarly, the E_a values for the degradation process of Mo-TG end capped PCL were found to be decreased for both the models.

4. Conclusions

The ROP of CL was effectively carried out by using novel Mo-TG initiator. The most important characteristics peaks such as C=O stretching (1722 cm^{-1}) and C-O-C (1183 cm^{-1}) ester linkage stretching modes were used to confirm the structure of PCL.

The assigned signals for alkoxy (4.08 ppm) and methylene protons (2.32 ppm) in the ^{1}H NMR spectrum were matched with the structure of PCL. The signals assigned for various groups of carbons in ^{13}C NMR spectrum were related to the structure of PCL. The particle size of the incorporated Mo-TG in the PCL matrix was measured to be in the range of 20-35 nm from the TEM image. Avrami and Mo's models suggested the 3D spherulitic crystal growth. It was further confirmed experimentally by polarized optical micrograph. Therefore, the theoretical results were in good agreement with the experimental results. It was observed that the crystallization temperature (T_c) and degradation temperature (T_d) of PCL were not constant under non-isothermal condition. The crystallization rate constant was increased with the increasing cooling rates. The energy of activation (E_a) for the decomposition of PCL was determined by four different kinetic models. The obtained values were found to be reliable with each other. The manufactures of biomedical products from PCL get benefited with the set of information provided by this study.

References

(1) K. Zoltowska, M. Sobczak, and E. Oledzka, *Molecules*, **20**, 2816 (2015).
(2) J. Khandare and T. Minko, *Prog. Polym. Sci.,* **31**, 359 (2006).
(3) M. A. Woodruff and D. W. Hutmacher, *Prog. Polym. Sci*., **35**, 1217 (2010).
(4) M. Sobczak, E. Olędzka, W. L. Kołodziejski, and R. Kuźmicz, *Polimery*, **52**, 411 (2007).
(5) L. S. Nair and C. T. Laurencin, *Prog. Polym. Sci*., **32**, 762 (2007).
(6) M. Labet and W. Thielemans, *Chem. Soc. Rev.,* **38**, 3484 (2009).
(7) W. Meelua, V. Buaown, R. Molloy, and W. Punyodom, *Adv. Mater. Res.,* **506**, 142 (2012).
(8) H. M. Sun, H. R. Li, C.S. Yao, Y. M. Yao, H. T. Sheng, and Q. Shen, *Chin. J. Chem.*, **23**, 1541 (2005).
(9) L. Kannammal, S. Palanikumar, B. Meenarathi, and R. Anbarasan, *J. Thermoplast. Compos. Mater.,* **30**, 1056 (2017).
(10) A. Sowkath, M. Ahmad, and R. Anbarasan, *Int. J. Chem. Biol. Sci.,* **1**, 1 (2014).
(11) J. M. Contreras, D. Medina, F. L. Carrasquero, and R. B. Contreras, *J. Polym. Res.,* **20**, 244 (2013).
(12) L. Liao, C. Zhang, and S. Gong, *Macromol. Rapid Commun.*, **28**, 1148 (2007).
(13) Z. X. Du, J. T. Xu, Y. Yang, and Z. Q. Fan, *J. Appl. Polym. Sci.*, **105**, 771 (2007).
(14) R. J. Pounder and A. P. Dove, *Polym. Chem.*, **1**, 260 (2010).
(15) V. Darcos, S. E. Habnouni, B. Nottelet, A. E. Ghaoui, and J. Coudane, *Polym. Chem.*, **1**, 280 (2010).
(16) J. Zhang and Z. Qiu, *Ind. Eng. Chem. Res.*, **50**, 13885 (2011).
(17) B. Wang, Y. Li, G. Weng, Z. Jiang, P. Chen, Z. Wang, and Q. Gu, *Compos. Sci. Technol.,* **96**, 63 (2014).
(18) L. S. Oliveira Pires, M. H. F. Vaz Fernandes, and J. M. Marques de Oliveira, *J. Therm. Anal. Calorim*., **134**, 2115 (2018).
(19) Y. Huang, H. Liu, P. He, L. Yuan, H. Xiong, and Y. Xu, *J. Appl. Polym. Sci.,* **116**, 2119 (2010).
(20) W. T. Chuang, U. S. Jeng, and H.,S. Sheu, *Macromol. Res*., **14**, 45 (2006).
(21) X. Qiao, W. Li, K. Sun, S. Xu, and X. Chen, *J. Appl. Polym. Sci.*, **111**, 2908 (2009).
(22) S. P. K. Vangala, A. Chaudhary, P. Tiwari, and V. Katiyar, *J. Energy Environ. Sustain*., **3**, 10 (2017).
(23) G. Sivalingam, R. Karthik, and G. Madras, *J. Anal. Appl. Pyrolys.,* **70**, 631 (2003).
(24) K. Chrissafis, *J. Therm. Anal. Calorim.*, **95**, 273 (2009).
(25) K. Chrissafis, G. Antoniadis, K.M. Paraskevopoulos, A. Vassiliou, and D. N. Bikiaris, *Compos. Sci. Technol*., **67**, 2165 (2007).
(26) M. Mucha, M. Tylman, and J. Mucha, *Polimery*, **60**, 11 (2015).
(27) M. W. Tzong and E. C. Chen, *Polym. Eng. Sci.,* **46**, 1309 (2006).
(28) Y. Li, C. Han, Y. Yu, L. Xiao, and Y. Shao, *J. Therm. Anal. Calorim.,* **131**, 2213 (2018).
(29) S. Achla, N. Maiti, and J. Jacob, *Int. J. Polym. Anal. Charact.,* **22**, 222 (2017).
(30) Y. Marquez, L. Franco, and J. Puiggali, *Thermochim. Acta*, **550**, 65 (2012).
(31) P. Tiwari and M. Deo, *AICHE. J.,* **58**, 505 (2012).
(32) M. M. Reddy, S. Vivekanandhan, M. Misra, S. K. Bhatia, and A. K. Mohantty, *Prog. Polym. Sci.,* **38**, 1653 (2013).
(33) S. Vyazovkin and N. Sbirrazzuoli, *Macromol. Rapid Commun.,* **27**, 1515 (2006).
(34) B. Meenarathi, P. Siva, S. Palanikumar, L. Kannammal, and R. Anbarasan, *Nanocomposites*, **2**, 98 (2016).
(35) L. Wang and J. Sheng, *J. Macromol. Sci. Part B: Phys.*, **44**, 31 (2014).
(36) J. Ahmed, G. Luciano, I. Schizzi, Y. Ali Arfat, S. Maggiore, T. Lidia, and A. Thai, *Thermochim. Acta*, **659**, 96 (2018).
(37) F. Shehzad, S. P. Thomas, and M. A. Al-Harthi, *Thermochim. Acta*, **589**, 226 (2014).
(38) K. Kawazu, S. Nakagawa, T. Ishizone, S. Nojima, D. Arai, K. Yamaguchi, and S. Nakahama, *Macromolecules,* **50**, 7202 (2017).
(39) A. Jancirani, V. Kohila, B. Meenarathi, A. Yellilarasi, and R. Anbarasan, *Bull. Mater. Sci.*, **39**, 1725 (2016).
(40) P. Demir, *J. Sci. Eng.,* **17**, 73 (2017).

